NJC

PAPER

View Article Online
View Journal | View Issue

Cite this: *New J. Chem.*, 2016, **40**, 7465

Adsorption of water induces a reversible structural phase transition and colour change in new nickel(II) macrocyclic complexes forming flexible supramolecular networks†

Brenda Lizette Ruiz-Herrera,[a] Marcos Flores-Álamo,[b] Rubén Alfredo Toscano,[c] Roberto Escudero[a] and Martha Elena Sosa-Torres*[b]

Received (in Montpellier, France) 23rd May 2016,
Accepted 21st June 2016

DOI: 10.1039/c6nj01621a

www.rsc.org/njc

Two novel 3D flexible supramolecular networks $[Ni_2(tpmc)(\mu\text{-}NO_3)](NO_3)_3(H_2O)_2[LiNO_3{\cdot}3H_2O]$ (**1**) and $[Ni_2(tpmc)(\mu\text{-}NO_3)]_2[Ni_2(tpmc)(\mu\text{-}NO_3)Li(NO_3)_2OH]_2(LiOH(H_2O)_3)_2(NO_3)_8(H_2O)_{13}{\cdot}nH_2O$ (**2**) (tpmc, 1,4,8,11-tetrakis-(2-pyridylmethylene)-1,4,8,11-tetraaza cyclotetradecane) were synthesized and characterized by spectroscopic and X-ray techniques. Their single crystal X-ray diffraction analysis showed that, in both compounds, nickel(II) ions are in an octahedral environment, due to an unusual binding mode of nitrate, acting either as a tetradentate ligand in **1**, or as a pentadentate ligand in **2**. The blue compound **1** adsorbs water leading to the violet compound **2**. Adsorption of water leads to a reversible crystal-to-crystal structural phase transition, from the monoclinic structure of **1** to the triclinic structure of **2**, a phenomenon that was corroborated by XRPD. This phase transition is accompanied by a reversible reaction of ligand exchange responsible for the color-change observed in the compounds, a property which might be useful for the development of molecular sensors. Adsorption–desorption isotherms recorded at low and high pressures indicated that **1** has capacity for adsorption of gases, such as dinitrogen, dioxygen, or carbon dioxide. Besides, dynamic water vapour isotherms confirm the chemisorption, highly selective for water vapor. This is the first time a Ni(II)–tpmc complex has been observed to be involved in a reversible gas adsorption process; furthermore, herein, we report the first crystal structures of six-coordinated nickel(II) complexes with tpmc.

Introduction

Numerous heterocyclic multidentate ligands and their transition metal complexes have been used as building blocks and templates for the design of functional materials.[1,2] Such supramolecular compounds include host–guest systems, molecular devices, self-assemblies, stimuli-sensitive materials, and nanoscale structures.[3] Within this, flexible solids are functional materials that can be either coordination or supramolecular networks. They possess flexible cavities that are able to adsorb a wide variety of molecules, performing reversible structural transformations, induced by the adsorption and removal of guest molecules.[4] In particular, flexible solids are involved in gas storage and sensing, in which water adsorption is especially important for technological applications, such as the design of water-delivering devices and adsorption-driven heat exchangers also known as thermal batteries, as well as their application as air-conditioning units in vehicles, or as dehumidifiers.[4,5]

We chose 1,4,8,11-tetrakis-(2-pyridylmethylene)-1,4,8,11-tetraazacyclotetradecane (tpmc) as base for our compounds. Tpmc is a macrocyclic ligand well known for its ability to form stable complexes with transition metals in lower oxidation states, *e.g.*, copper(II), cobalt(II) and nickel(II), among others.[6–10] In these binuclear complexes, the metal ions remained exo-coordinated from the macrocycle, where tpmc can adopt either a chair or boat conformation depending on the metal ion and the nature (mono- or polydentate) of the secondary ligand bound to the metal centers.[6,7] Fig. 1 shows the tetraaza macrocycle tpmc and its conformational structures adopted in binuclear compounds.

Like other tetraaza macrocyclic ligands, tpmc coordinates each metal ion with the two cyclam ring nitrogens and with two

[a] *Instituto de Investigaciones en Materiales, Universidad Nacional Autónoma de México, Ciudad Universitaria, Cd. Mx., 04510, México*
[b] *Departamento de Química Inorgánica y Nuclear, Facultad de Química, Universidad Nacional Autónoma de México, Ciudad Universitaria, Cd. Mx., 04510, México*
[c] *Instituto de Química, Universidad Nacional Autónoma de México, Ciudad Universitaria, Cd. Mx., 04510, México. E-mail: mest@unam.mx*

† Electronic supplementary information (ESI) available: Additional infrared spectra, further representation of crystal structures, and additional measurements related to water adsorption. CCDC 1406400 and 1406401. For ESI and crystallographic data in CIF or other electronic format see DOI: 10.1039/c6nj01621a

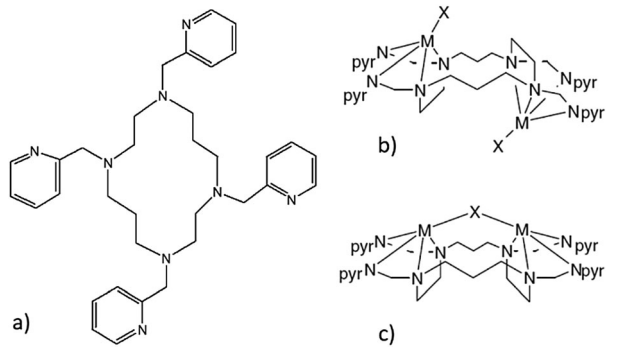

Fig. 1 (a) Representation of the 1,4,8,11-tetrakis-(2-pyridyl methylene)-1,4,8,11-tetraazacyclotetradecane (tpmc), (b) its chair structure and (c) boat structure.

donor atoms of the pendant groups, leaving one of the axial positions open for a secondary ligand, while the other position is sterically blocked by the pendant groups. This arrangement explains the preference for five-coordinated structures.[7,11,12] Nevertheless, six-coordinated structures of metal complexes with tetraaza macrocycles become feasible when using an appropriate secondary ligand. For example, Co(II) and Ni(II) complexes with 1,4,8,11-tetrakis-(2-aminoethyl)-1,4,8,11-tetraazacyclotetradecane (taec) show octahedrally distorted metal sites, with carbonate as a secondary ligand. Here, the carbonate anion acts as a bridging ligand in a symmetrically bidentate way.[11,12] So far, crystal structures of analogous tpmc complexes have not been reported, however, infrared and electronic spectra of $[Co_2CO_3(tpmc)](ClO_4)_2{\cdot}2H_2O$ and $[Co_2CO_3(tpmc)](BF_4)_2{\cdot}2H_2O$ suggest the presence of six-coordinated Co(II) sites. Surprisingly, in view of the numerous crystal structures of $[M_2(tpmc)L]$ complexes, structures of the corresponding Ni(II) complexes have not been reported to date,[13a] even though Ni(II)–tpmc complexes are known since many years.[9]

Here we describe the functional and structural characterization of two new Ni_2(tpmc) complexes **1** and **2**, with nitrate as a secondary ligand, stabilizing hexa-coordinated Ni(II) centers. The compounds form flexible supramolecular solids involved in a reversible adsorption–desorption water process. The change in the hydrogen bonding network caused by the inclusion of water induced a structural phase transition, from monoclinic to triclinic, accompanied by a reversible ligand exchange. This results in a remarkable color change, from blue (complex **1**) to violet (complex **2**), a property which might be useful for the development of molecular sensors.

Experimental

Materials and methods

Commercially available reagents were used without further purification, gases were from Praxair. Fourier transform infrared spectra were recorded on a Perkin-Elmer 400 FT-IR/FT-FIR spectrophotometer, over the range 4000 to 400 cm^{-1} (attenuated total reflectance mode), and for the range of 600 to 50 cm^{-1} (polyethylene pellet windows). Electronic absorption spectra were measured on a Cary – 5E Varian spectrometer over the range 40 000–4000 cm^{-1} in diffuse reflectance mode. Elemental analyses were carried out on a Perkin-Elmer 2400 microanalyser, using L-cystine as standard.

Synthesis of tpmc

The ligand 1,4,8,11-tetrakis-(2-pyridylmethylene)-1,4,8,11-tetraazacyclotetradecane (tpmc) was prepared following a reported procedure; its characterization by ^{1}H-NMR and elemental analysis agree with reported values.[10]

Synthesis of $[Ni_2(tpmc)(\mu\text{-}NO_3)](NO_3)_3(H_2O)_2[LiNO_3{\cdot}3H_2O]$: 1. A solution of tpmc (0.5 g, 0.88 mmol) and LiOH (0.048 g, 2.0 mmol) in anhydrous ethanol was stirred under nitrogen gas flux for 10 minutes. Then, a solution of $Ni(NO_3)_2{\cdot}6H_2O$ (0.52 g, 1.77 mmol) in anhydrous ethanol was added dropwise to the ligand solution over a period of 1 h. The mixture was refluxed under nitrogen for 20 h. The blue precipitate was collected by filtration, washed with a minimum amount of dry dichloromethane, and finally dried under a dinitrogen atmosphere, giving the blue complex **1**, $[Ni_2(tpmc)(\mu\text{-}NO_3)](NO_3)_3{\cdot}(H_2O)_2[LiNO_3{\cdot}3H_2O]$; anal. calc. for $Ni_2C_{34}N_{13}H_{54}O_{20}Li$ (%): C, 37.49; H, 4.99; N, 16.72; found: C, 37.76 ± 1.79; H, 3.63 ± 1.37; N, 15.59 ± 0.56. The presence of lithium, which comes from the reactants, was confirmed by the lithium flame test.[14]

Synthesis of $[Ni_2(tpmc)(\mu\text{-}NO_3)]_2[Ni_2(tpmc)(\mu\text{-}NO_3)Li(NO_3)_2OH]_2(LiOH(H_2O)_3)_2(NO_3)_8(H_2O)_{13}{\cdot}nH_2O$: 2. Exposure of complex **1** to ambient laboratory conditions leads to the violet complex **2**: $[Ni_2(tpmc)(\mu\text{-}NO_3)]_2[Ni_2(tpmc)(\mu\text{-}NO_3)Li(NO_3)_2OH]_2(LiOH(H_2O)_3)_2$-$(NO_3)_8(H_2O)_{13}{\cdot}nH_2O$; where n = 32. Anal. calc. for $Ni_8C_{136}N_{48}$-$H_{282}O_{103}Li_4$ (%): C, 34.49; H, 6.00; N, 14.19; found: C, 34.63 ± 0.65; H, 4.80 ± 0.41; N, 14.14 ± 0.26.

Additionally, **2** was obtained by exposing **1** to deuterated water vapour, using deuterium oxide (99.9 atom% D) from Aldrich.

X-ray diffraction (XRD) crystal analysis

Suitable crystals of complex **1** were obtained from the original reaction mixture prior to the filtration step. A small amount of the solution was kept at room temperature to allow slow evaporation, giving blue crystals of complex **1**. After an aging period, the blue crystals turned into the violet crystals of complex **2**.

The structure of complex **1** was determined at 120 K on an Oxford Diffraction Gemini "A" diffractometer, equipped with a CCD area detector, a sealed tube X-ray radiation source ($\lambda_{MoK\alpha}$ = 0.71073 Å), and a graphite monochromator. The CrysAlisPro and CrysAlis RED software packages were used for data collection and data integration.[15] Analysis of the integrated data did not reveal any crystal decay. The final cell constants were determined by the global refinement of 5583 ($3.462 < \theta < 29.565^\circ$) and collected data were corrected for absorption effects.

The structure of complex **2** was determined on a Bruker Smart Apex diffractometer, using Mo-Kα radiation, a graphite-monochromator, and ω scans at 150 K. The intensities were integrated using SAINT, and absorption correction and scaling were performed using SADABS.[16]

Both structures were solved using the program SHELXS97; the full-matrix least-squares refinement was achieved using SHELXL97 for complex **1** and SHELXL-2014 for complex **2**.[17]

All atoms except hydrogen were refined anisotropically. The hydrogen atoms of water were located in a difference Fourier map and refined isotropically with $U_{iso}(H) = 1.5U_{eq}$ for (O). H atoms attached to C atoms were placed in geometrically idealized positions and refined by a riding model with isotropic displacement parameters associated with the parent carbon atoms. ORTEP-3 for Windows was employed for molecular graphics.[18] Finally, the programs CCDC MERCURY and Diamond 4.0 were used to prepare the material for publication.[19]

Many efforts to refine the structure of compound **2** in the triclinic space group $P\bar{1}$ were unsuccessful, that is why the structure was refined in the triclinic space group $P1$, which reveals a clear overall centrosymmetric arrangement, quantified by the PLATON-ADDSYM routine in 92%. The presence of an additional (Non) crystallographic glide plane between Ni cations was also detected by the PLATON-NONSYM routine.

X-Ray powder diffraction (XRPD) analysis

Data were obtained on a Bruker D-8 Discover diffractometer with the Bragg–Brentano θ–θ configuration, equipped with a Cu-Kα radiation source, a Ni (0.5%) Cu-Kβ filter in the secondary beam, and a one-dimensional position-sensitive silicon strip detector (Bruker, Lynxeye). XRPD patterns were obtained under vacuum in a sealed sample holder at 298 K; this temperature was gradually increased to 353 K using an Anton-Paar HTK 1200N high-temperature oven chamber. In all cases, the diffraction intensity as a function of 2θ angle was measured between 4.001 and 109.98°, with a 2θ step of 0.019447°, for 264 s per point. Diffraction patterns were indexed with software EXPO2014.[20]

Analysis of functional properties

The complexes were investigated by thermogravimetric analysis, BET adsorption–desorption and water-vapour isotherms and scanning electron microscopy coupled to energy-dispersive X-ray spectroscopy (SEM-EDS).Thermogravimetric analyses were performed under dinitrogen (grade 5.0), with a heating rate of 5 °C min^{-1} (278 K min^{-1}) in a thermobalance Mettler-Toledo model TGA/SDTA851^e.

Isotherms at low relative-pressure, under nitrogen, were acquired on a Bel-Japan Minisorp II at 77 K, by using a multipoint technique. Samples were degassed at 353 K for 20 h under vacuum prior to the analysis. Data were analysed applying the Brunauer–Emmett–Teller (BET) and the Barrett–Joyner–Halenda (BJH) models.[21] Isotherms at high pressure, under CO_2, were obtained on a volumetric Belsorp-HP instrument from Bel-Japan. The equipment performs additional degassing of the sample by applying vacuum. Experiments were performed between atmospheric and 4.5 MPa pressure, at 303.5 K.

Dynamic water adsorption/desorption studies were carried out on a Q5000SA thermobalance from TA Instruments (associated error of 0.1 wt%), equipped with a humidity and temperature controlled chamber (associated error of 0.1% of relative humidity). Prior to the measurements the samples were degassed (vacuum, 353 K, 20 h). The measurements were performed using distilled water and carrier gases dinitrogen (grade 4.8), carbon dioxide (3.0) and dioxygen (2.6). The total gas flow rate was 100 mL min^{-1}, and the relative humidity (RH) percentages were automatically controlled by the instrument.

The morphology and elemental composition of complexes were determined on a JEOL JMS-7600F SEM-EDS instrument.

Results and discussion

Reversible switching between compounds 1 and 2

The reaction between $Ni(NO_3)_2{\cdot}6H_2O$ and tpmc in anhydrous ethanol produced the blue Ni(II) complex **1** when performed under dinitrogen. Upon exposure to air (ambient laboratory environment) complex **1** was transformed to the violet complex **2**. To obtain a further insight into these findings, the reaction was repeated several times recovering the product under different atmospheres: carbon dioxide, dioxygen or water vapor. It was found that the observed colour-change is the result of an adsorption phenomenon of water vapour, a phenomenon that is reversible even after several cycles. Moreover, it is easy to cause interchange between the two complexes; *i.e.* **1** can be obtained by warming **2** at 353 K for 2 h in a vacuum furnace, and **2** can be obtained by exposing **1** to the environment. Fig. S1 (ESI†) shows a schematic representation of the described process.

Hexa-coordinated nickel(II) complexes with tpmc

The electronic solid state reflectance spectra of both complexes **1** and **2** (Fig. 2) revealed features consistent with an octahedral environment of Ni(II) (d^8).[22] For complex **1**, the first maximum at 968 nm (10 330 cm^{-1}) corresponds to the transition $^3A_{2g} \rightarrow {}^3T_{2g}$ (F) (ν^1); the second, at 575 nm (17 402 cm^{-1}), to $^3A_{2g} \rightarrow {}^3T_{1g}$ (F) (ν^2); and the third, at 375 nm (26 667 cm^{-1}), to $^3A_{2g} \rightarrow {}^3T_{1g}$ (P) (ν^3). In the case of compound **2**, the corresponding transitions are observed at 952 nm (10 507 cm^{-1}) with shoulder peaks at 890 nm (11 231 cm^{-1}), 569 nm (17 575 cm^{-1}) and 368 nm (27 152 cm^{-1}). The maxima of complex **2** are slightly shifted to higher energies consistent with the observed colour change from blue to violet.

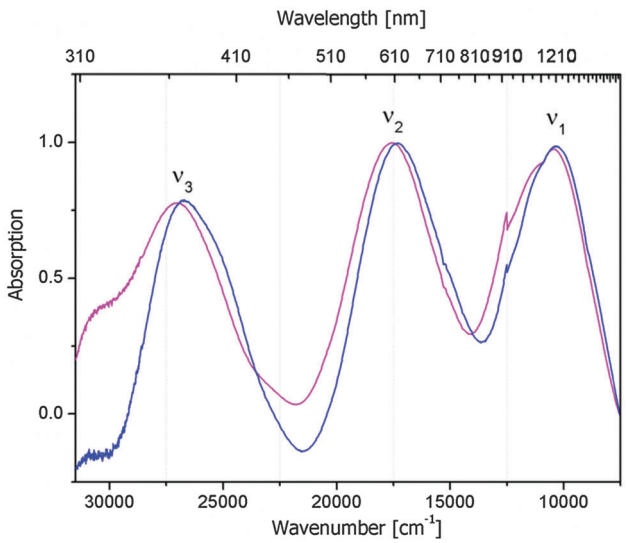

Fig. 2 Electronic spectra of Ni(II) complexes: **1** (blue line) and **2** (violet line).

Ni(II)–tpmc complexes differentiated by infrared spectroscopy

Mid-infrared spectra (vs: very strong; s: strong; m: medium; w: weak intensity) of complexes **1** and **2** (Fig. S2, ESI†) revealed maxima at 2924 cm^{-1} (m) and 2891 cm^{-1} (m) for $\nu(CH_2)$, at 1610 cm^{-1} (s) and 1574 cm^{-1} (m) for $\nu(C{=}N)$, as well as showed a maximum characteristic of mono-substituted pyridines at 760 cm^{-1} (s).[23] These maxima are shifted relative to those of the free ligand, in agreement with previously reported data for tpmc complexes.[7,9]

Besides, there are maxima which can be assigned to a coordinated nitrate anion,[24] at 1483 cm^{-1} (vs) [$\nu_s(NO_3)$], 1277 cm^{-1} (vs) [$\nu_1(NO_3)$] and 1027 cm^{-1} (s) [$\nu_2(NO_3)$] for complex **1**, compared to 1511 cm^{-1} (vs) [$\nu_s(NO_3)$], 1272 cm^{-1} (vs) [$\nu_1(NO_3)$] and 1025 cm^{-1} (s) [$\nu_2(NO_3)$] for **2**. The difference $\Delta(\nu_s–\nu_1)(NO_3)$ of 206 cm^{-1} (complex **1**) and 239 cm^{-1} (complex **2**) originates from a chelating nitrate ligand, whereas the maximum at 1335 cm^{-1} (vs) is assigned to nitrate anions not involved in metal binding.[23,24]

Finally, the mid-IR spectra of complexes **1** and **2** differ with regard to characteristic bands resulting from lattice water.[23] Compound **2** shows a maximum at 3400 cm^{-1} which is assigned to the stretching H–O–H vibration mode, with the corresponding bending vibration maximum at 1640 cm^{-1}. These features are absent in the spectrum of compound **1**.

Far infrared spectra of complexes **1** and **2** (Fig. 3) show a band centered at 270 cm^{-1} [ν_s(M–O, NO_3)] consistent with a coordinated nitrate,[23,24] the second maximum at 420 cm^{-1} has been assigned to [ν_s(M–N), tpmc].[13b] In the spectrum of complex **2** there are two additional maxima at 537 and 574 cm^{-1}, which are absent in the spectrum of complex **1**.

The discussion on the origin of these bands is found to be controversial in the literature, they were assigned either to the M–O bond of a coordinated water molecule (ν(M–O,H_2O)) or to the M–O bond of a coordinated nitrate anion (ν(M–O, NO_3^-)).[24] In order to assign these bands, complex **2** was produced by the exposure of complex **1** to D_2O vapour.

The resulting mid-infrared spectrum of deuterated complex **2** (Fig. S3a, ESI†) revealed the expected shift from 3400 to 2523 cm^{-1} for the D–O–D stretching vibration.[23] While in the far infrared spectrum (Fig. S3b, ESI†) none of the bands were shifted. Thus, the bands at 537 and at 574 cm^{-1} were assigned to coordinated nitrates.

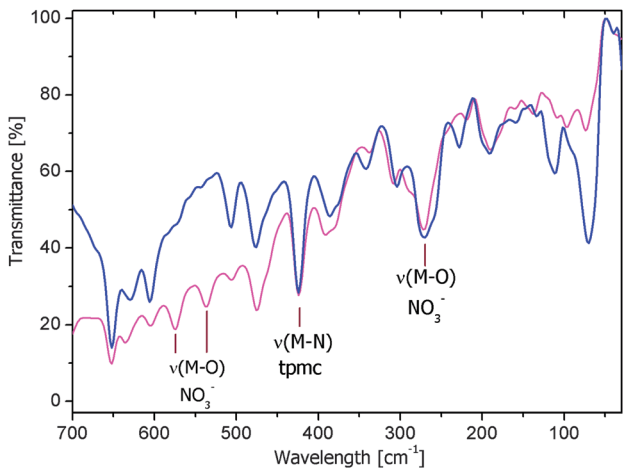

Fig. 3 Far-infrared spectra of Ni(II) complexes: **1** (blue line) and **2** (violet line), showing the position and assignment of the individual bands.

Crystal structures of complexes 1 and 2

Blue crystals of **1**, suitable for single-crystal X-ray diffraction, were obtained directly from the reaction mixture. When these crystals were exposed to ambient laboratory conditions for several days, the violet crystals of **2** were obtained. Crystallographic parameters are compiled in Table 1.

Ni(II) complex **1** crystallized in a monoclinic structure with a space group $P2_1/n$. The asymmetric unit was formed by one $[Ni_2(tpmc)(\mu\text{-}NO_3)]^{3+}$ cation, three nitrate anions, two water molecules and one $Li(NO_3)(H_2O)_3$ unit (Fig. S4, ESI†).

A perspective view of the molecular structure of the $[Ni_2(tpmc)(\mu\text{-}NO_3)]^{3+}$ cation in compound **1** is shown in Fig. 4 (left). Nickel ions are bridged by a tpmc ligand and by a nitrate. As in previous tpmc complexes,[7–10] the octadentate ligand is coordinated to the two nickel(II) ions through the nitrogen atoms of the four pendant pyridine rings and through the four nitrogen atoms of the macrocycle. Metal centres are exo-coordinated, out of the cyclam ring which adopts an SRSR(RSRS) configuration. Added to this, the coordination mode of the nitrate anion gives an octahedral geometry for the nickel atoms, consistent with the electronic spectrum of the compound. In this environment one macrocyclic amine, one methylpyridine and two of the oxygen atoms of the nitrate group occupy an equatorial plane, while the remaining macrocyclic amine and methylpyridine pendant occupy the apical positions of each nickel(II) ion. The found Ni–N bond lengths in complex **1**, 2.049(3) to 2.147(3) Å, are within the expected range, according to the bond lengths of analogous cobalt and copper complexes.[7–10,25] Table S1 (ESI†) lists the selected bond distances and angles for complex **1**.

A further description of the nitrate ligand indicates that it behaves as a tetradentate bridging ligand, connecting the two nickel(II) centres in a bis-bidentate way.[26] This can be described as μ^2-nitrate-1κ^1O,2κ^1O,3κ^2O, which means two oxygen atoms from the nitrate ligand are coordinated each to one of the two nickel(II) ions, while the third oxygen is bonded to both metal centres.[27]

There are few examples of this coordination by a nitrate anion.[26,28,29] An equivalent coordination mode was observed for a carbonate anion in the binuclear nickel(II) complex with the ligand taec,[12] in which the μ-carbonate-bridge ligand is bound to the metals centres by its oxygens, in the same way as our nitrate bridges the nickel(II) ions. The distorted octahedral geometry of the metal centres in complex **1** results from the presence of this symmetrically bidentate ligand. The O–Ni–O angles (62.15(9) and 62.69 (9)°) in complex **1** show the deviation from the ideal octahedral geometry. Table S1 (ESI†) compiles the main bond lengths and angles of compound **1**.

The lithium site in $Li(NO_3)(H_2O)_3$ present in complex **1** shows a pentacoordinated Li^+ cation in a distorted trigonal bipyramidal geometry, formed by three water molecules and one chelating nitrate anion. Such coordination is rather uncommon for lithium

Table 1 Crystal data and structure refinement for complexes **1** and **2**

Compound	**1**	**2**
Empirical formula	$C_{34}H_{54}LiN_{13}Ni_2O_{20}$	$C_{136}H_{218}Li_4N_{48}Ni_8O_{71}$
Formula weight	1089.26	4159.01
Temperature	120(2) K	150(2) K
Crystal system	Monoclinic	Triclinic
Space group	$P2_1/n$	$P1$
Unit cell dimensions	a = 11.2417(7) Å b = 18.3142(11) Å c = 22.6389(13) Å α = 90° β = 101.822(6)° γ = 90°	a = 11.2964(8) Å b = 18.8819(14) Å c = 20.7624(13) Å α = 87.453(5)° β = 89.238(4)° γ = 83.960(5)°
Volume	4562.1(5) Å^3	4399.5(5) Å^3
Z	4	1
Density (calculated)	1.586 Mg m^{-3}	1.570 Mg m^{-3}
Absorption coefficient	0.918 mm^{-1}	0.944 mm^{-1}
F(000)	2272	2174
Crystal size/colour/shape	0.58 × 0.20 × 0.19 mm/blue/prism	0.383 × 0.229 × 0.196 mm/violet/prism
Theta range for data collection	3.462 to 29.565°	1.432 to 27.641°
Index ranges	$-11 \le h \le 14$, $-12 \le k \le 23$, $-29 \le l \le 31$	$-14 \le h \le 11$, $-24 \le k \le 24$, $-26 \le l \le 26$
Reflections collected	23 469	43 154
Independent reflections	10 724 [R(int) = 0.0323]	28 357 [R(int) = 0.0498]
Completeness to theta	99.8% (θ = 25.242°)	99.3% (θ = 25.242°)
Refinement method	Full-matrix least-squares on F^2	Full-matrix least-squares on F^2
Data/restraints/parameters	10 724/0/655	28 357/83/2524
Goodness-of-fit on F^2	1.040	1.015
Final R indices [$I > 2\sigma(I)$]	R_1 = 0.0586, wR_2 = 0.1470	R_1 = 0.0624, wR_2 = 0.1551
R indices (all data)	R_1 = 0.0825, wR_2 = 0.1661	R_1 = 0.0844, wR_2 = 0.1699
Extinction coefficient	n/a	—
Absolute structure parameter	—	0.423(12)
Largest diff. peak and hole	1.979 and −0.912 e Å^{-3}	0.699 and −1.998 e Å^{-3}

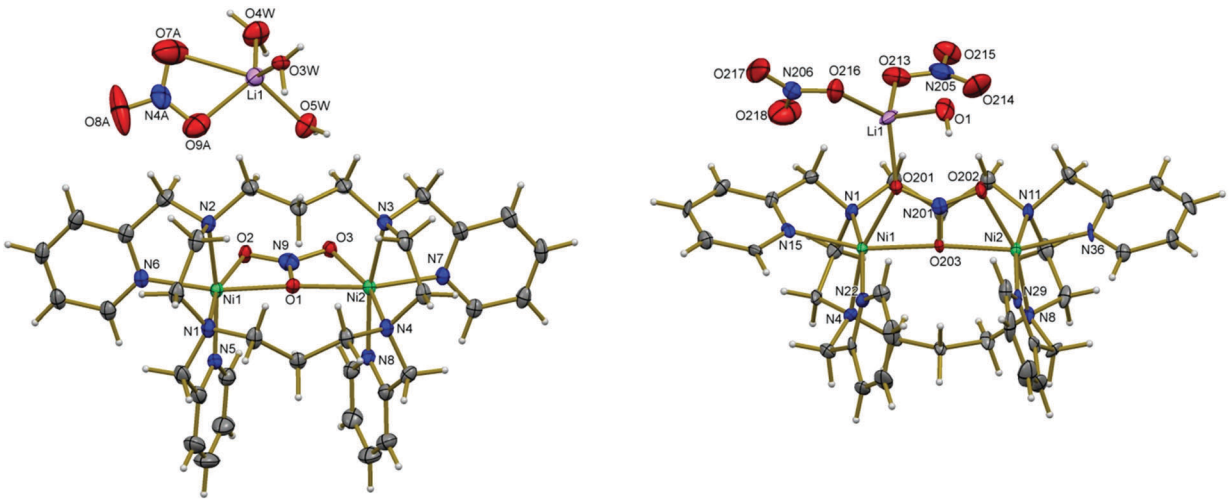

Fig. 4 Structural comparison between cations present in compounds **1** (left) and **2** (right). A perspective view of the molecular structures, C (black); H (white); O (red); N (blue); Ni (green) and Li (pink). Thermal ellipsoids are shown at the 50% probability level.

and has mostly been observed in organometallic lithium compounds[30–32] and in LiB_6O_9F, the first reported lithium fluorooxoborate.[33] Accordingly, the mean Li–O distance (1.921(8) to 2.429(9)) in complex **1** is in agreement with the distances observed in these previously reported compounds (see Table S2, ESI†).

Fig. 5 shows the crystal lattice of **1**, where the intermolecular interactions through hydrogen bonding can be observed around the binuclear nickel complexes. In general, these interactions form a $D_2^2(5)$, $D_2^2(7)$ and $R_2^2(8)$ graphical set,[34] corresponding to chains and rings where two donor atoms and two acceptors form the hydrogen bonding, leading to a three-dimensional supramolecular architecture that gives structural stability to the network of complex **1**. Table 2 summarizes the main hydrogen bonding interactions present in compound **1**.

The exposure of the blue crystals of complex **1** to ambient conditions produced the violet crystals of complex **2**, which crystallizes in a triclinic structure with the space group $P1$.

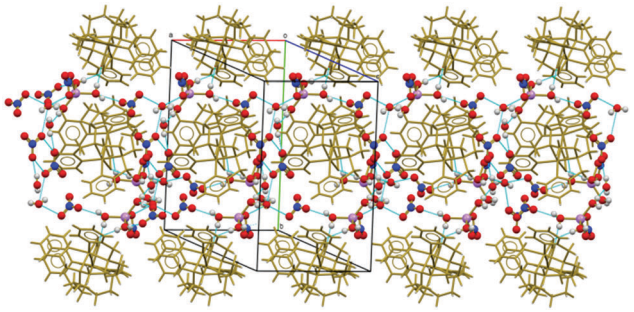

Fig. 5 Crystal lattice of complex **1** along the plane *a*–*b*. Intermolecular hydrogen bond interactions are marked in green.

Table 2 Hydrogen bonding interactions in complexes **1** and **2**

Donor–H···Acceptor	D–H [Å]	H···A [Å]	D···A [Å]	D–H ··· A [°]
Complex **1**				
O(3W)–H(3WA)···O(2)[a]	0.80(10)	1.92(10)	2.721(4)	172(9)
O(3W)–H(3WB)···O(1A)[b]	0.78(10)	2.11(9)	2.842(5)	158(10)
O(4W)–H(4WA)···O(11A)[c]	0.96(9)	1.88(9)	2.825(6)	166(8)
O(5W)–H(5WB)···O(3)[a]	0.85(9)	1.98(9)	2.824(4)	173(9)
Complex **2**				
O(1)–H(1)···O(227)	0.818(13)	2.07(5)	2.815(14)	150(9)
O(7)–H(7C)···O(215)	0.849(13)	2.27(4)	2.851(12)	125(4)
O(4)–H(4)···O(211)	0.826(13)	1.97(3)	2.751(9)	157(7)
O(10)–H(10C)···O(210)	0.852(13)	1.86(3)	2.684(10)	163(10)
O(13)–H(13D)···O(215)[d]	0.851(13)	2.26(11)	2.977(14)	141(15)
O(16)–H(16A)···O(217)[d]	0.848(13)	2.08(3)	2.910(13)	165(11)
O(1)–H(1)···O(227)	0.818(13)	2.07(5)	2.815(14)	150(9)

Symmetry transformations used to generate equivalent atoms: (a) $-x+2$, $-y+1$, $-z+1$; (b) $x+1/2$, $-y+3/2$, $z+1/2$; (c) $-x+3/2$, $y+1/2$, $-z+3/2$; and (d) $x-1$, y, z.

The unit cell of complex **2** (Fig. S5, ESI†) consists of two types of binuclear Ni(II) cations, two lithium entities: $Li(OH)(H_2O)_3$, eight nitrate anions and thirteen water molecules. Table 1 summarizes crystallographic parameters.

One of the nickel cations in compound **2** is exactly the same as that one described in **1**, corresponding to the molecule $[Ni_2(tpmc)(\mu\text{-}NO_3)]^{3+}$. In the second cation, the mode of coordination of tpmc and the nitrate ligand is retained, but it differs by the presence of a lithium coordinated to one of the oxygens (O201) of the bridging nitrate, resulting in the non-equivalence of the nickel ions. The interatomic distance Li(1)–O(201) is 1.972(17) Å corresponding to a covalent bond. The tetrahedral geometry of this lithium attached to the oxygen of the nitrate-bridging ligand is completed by one hydroxyl and two nitrate anions. The second cation in compound **2** then corresponds to the molecule $[Ni_2(tpmc)(\mu\text{-}NO_3)Li(NO_3)_2OH]^{+}$ shown in Fig. 4 (right).

In a similar way, in the carbonato-bridged cobalt(II)–taec complex, a sodium ion is located in close proximity to one of the carbonate oxygens, suggesting a Na–O bond.[12]

The nitrate in the second cation acts as a pentadentate bridging ligand described as μ^3-nitrate-1κ^1O,2κ^2O,3κ^2O.[27] This is the first observation of this coordination mode for nitrate (see Table S1, ESI†).

It is worth mentioning that the incorporation of the lithium entity into the coordination sphere of nickel in complex **2** changes its electronic environment, resulting in the observed colour change.

The adsorption of water induces the coordination of lithium entities towards the bridging nitrate, a process that is completely reversible when water is removed. This switching in the coordination sphere has been described as a reaction of ligand exchange.[35]

Crystal lattices of complexes **1** and **2** are stabilized mainly by intermolecular interactions of hydrogen bonding. The structure of **1** has cavities and channels along the network. When the adsorption process takes place, water molecules occupy these positions, causing a distortion and expansion of the original frame, giving rise to a new lattice in complex **2**.

The crystal lattice of **2** contains water molecules distributed in open channels along the *c* axis (Fig. 6). These interactions, summarized in Table 2, correspond to hydrogen bonds of types $D_2^2(8)$, $D_2^2(9)$ and $R_2^2(8)$.[34] An additional representation of the crystal lattice of compound **2** is shown in Fig. S6 (ESI†), where the molecules involved in the hydrogen bonding are emphasised in order to get a better perspective of these supramolecular interactions.

The hydration process modifies the supramolecular networks promoting the reversible phase transition from monoclinic in **1** to a triclinic structure in **2**. Fig. 7 shows the reaction of reversible ligand exchange and compares different views of the supramolecular frameworks of complexes **1** and **2**, underlining the importance of lithium units in the stabilization of the crystal lattices and its role in the reversible reaction of ligand exchange upon adsorption of water. Fig. 8 presents a plausible motion of molecules involved in the ligand exchange reaction.

The non-equivalence of nickel atoms derived from this water-induced ligand-exchange process explains the shift to higher

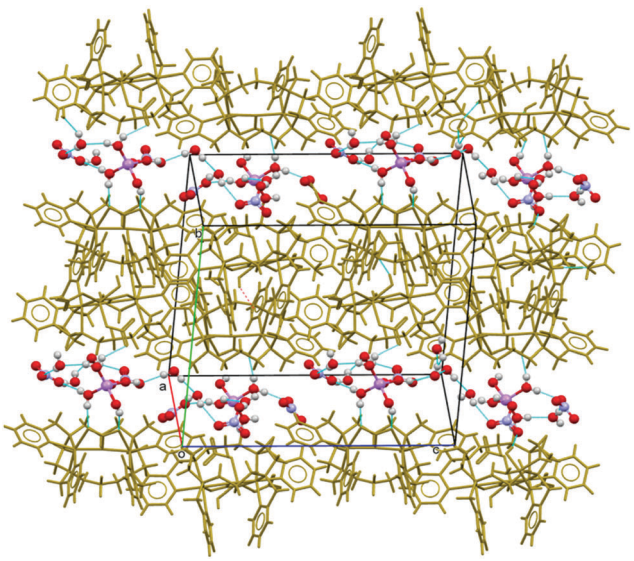

Fig. 6 Crystal lattice of complex **2**. Intermolecular hydrogen bond interactions are marked in green.

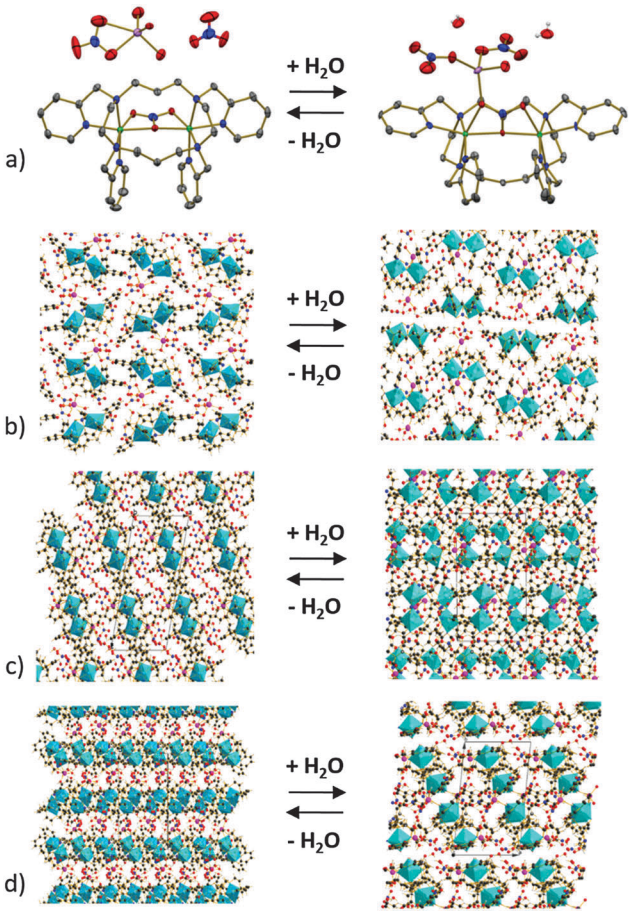

Fig. 7 Reversible ligand exchange and structural phase transition induced by water adsorption. (a) Interconversion between the Ni(II)–tpmc cations present in compounds **1** and **2**. A perspective view of the supramolecular network of complexes **1** and **2** along the *a* axis (b); *b* axis (c), and *c* axis (d). Nickel polyhedra are marked in green.

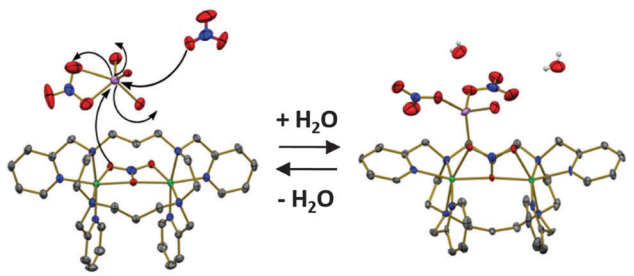

Fig. 8 Drawing of a possible motion of molecules involved in the ligand exchange reaction.

energies of the bands in the electronic spectrum of compound **2** (Fig. 1) and the observed colour change. This also explains the differences observed in the infrared spectra of the compounds. The shift of the observed bands to higher energies for complex **2**, at 1511 cm^{-1} [$\nu_s(NO_3)$], 1272 cm^{-1} (vs) [$\nu_1(NO_3)$] and 1025 cm^{-1} (s) [$\nu_2(NO_3)$] (Fig. S2, ESI†), is in agreement with a new coordination mode of the nitrate. On the other hand, in the far region (Fig. 3), the bands at 537 and 574 cm^{-1}, only present in the spectrum of compound **2**, correspond to a second vibration mode of the oxygen atom of the nitrate coordinated simultaneously to nickel and lithium atoms. These bands disappear when the sample is dehydrated, leading to compound **1**, and reappear upon adsorption of water, giving evidence for this reversible structural change.

Powder X-ray diffraction

As stated by single crystal X-ray diffraction analysis, the binuclear nickel(II) complexes reported here undergo a crystalline-to-crystalline transformation induced by adsorption of water. This dynamic structural behaviour was verified by powder X-ray diffraction (XRPD).

When complex **2** is heated in a vacuum furnace at 353 K for two hours, complex **1** is obtained, which remains dehydrated for several days if kept under a nitrogen atmosphere in a desiccator. When **1** was exposed to ambient conditions compound **2** was obtained almost immediately. Fig. 9 shows the XRPD patterns of the described samples. The identity of each compound was confirmed by infrared spectroscopy and elemental analysis. These results indicate a phase transition from a triclinic structure for compound **2** (anal. calc. (%): C, 34.49; H, 6.00; N, 14.19; found: C, 34.63 ± 0.65; H, 4.80 ± 0.41; N, 14.14 ± 0.26), (Fig. 9a) to another crystalline structure, corresponding to compound **1** (anal. calc. (%): C, 37.49; H, 4.99; N, 16.72; found: C, 37.76 ± 1.79; H, 3.63 ± 1.37; N, 15.59 ± 0.56), (Fig. 9b). The original crystalline phase was restored after the rehydration process (Fig. 9c) producing complex **2** $[Ni_2(tpmc)(\mu\text{-}NO_3)]_2[Ni_2(tpmc)(\mu\text{-}NO_3)\text{-}Li(NO_3)_2OH]_2(LiOH(H_2O)_3)_2(NO_3)_8(H_2O)_{13}\cdot nH_2O$, where n = 20. (Anal. calc. C, 36.15; H, 5.75; N, 14.87; found: C, 36.23 ± 0.02; H, 5.10 ± 0.02; N, 14.96 ± 0.025).

Fig. 10 shows the structural phase transition by comparison between indexed reflections of the diffraction patterns of complexes **1** and **2**. All the reflections were assigned.[20]

Microstructural characterization and description of the sorption phenomenon

Thermogravimetric (TG) and differential thermogravimetric (DTG and DTA) analyses were performed for **1** and **2**. Fig. 11 shows the

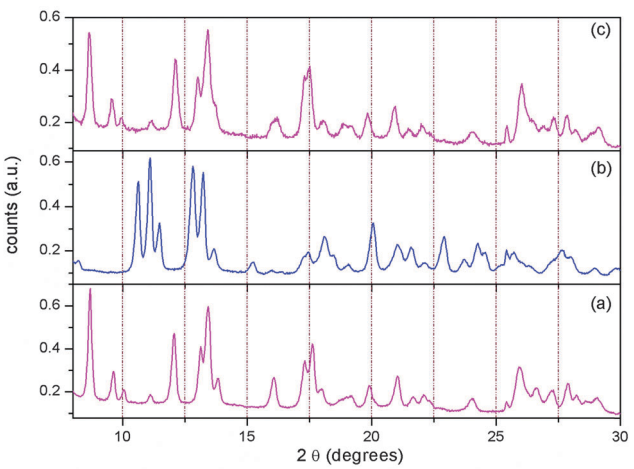

Fig. 9 XRPD patterns for complex **2** (a), complex **1** (b) and the recovered complex **2** (c).

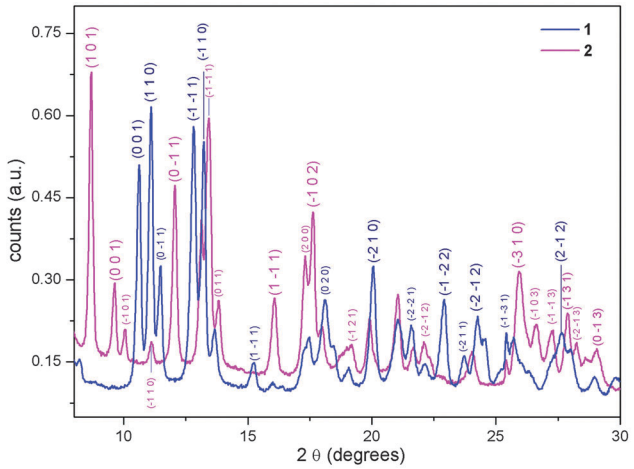

Fig. 10 Assignment of the reflections in the XRPD patterns for complexes **2** and **1**, and a comparison between them.

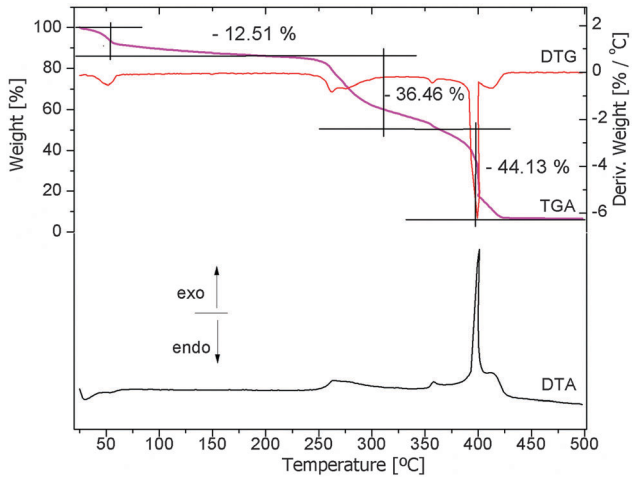

Fig. 11 Thermal analyses of **2** run under N_2 at 5 °C min^{-1}.

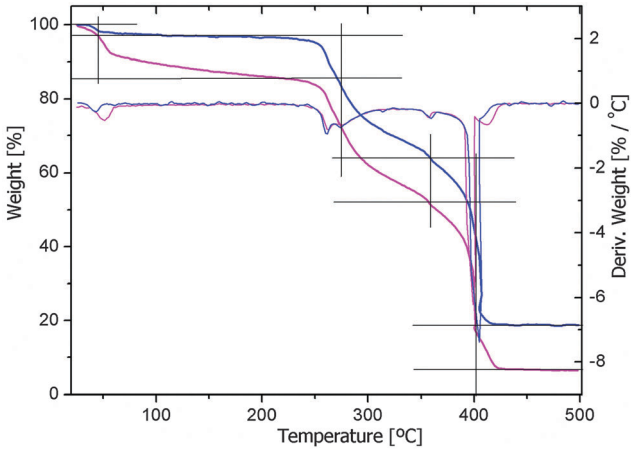

Fig. 12 Comparison between thermogravimetric and differential thermogravimetric curves for compounds **1** (blue line) and **2** (violet line). Measurements run under N_2 at 5 °C min^{-1}.

decomposition pattern of compound **2**. The first transition corresponds to the loss of 12.51 wt% (30–180 °C) assigned to 32 molecules of water (calc. 12.20%), confirming the formula: $[Ni_2(tpmc)(\mu\text{-}NO_3)]_2[Ni_2(tpmc)(\mu\text{-}NO_3)Li(NO_3)_2\ OH]_2(LiOH(H_2O)_3)_2(NO_3)_8(H_2O)_{13}{\cdot}32H_2O$, as determined by elemental analysis. This transition corresponds to the loss of adsorbed water. At the beginning (≈50 °C) an abrupt change is observed, corresponding to the loss of the most superficial water. As temperature rises, the chemisorbed water is lost gradually until all water is desorbed at 180 °C.

The second transition corresponds to the loss of 36.46% (215–350 °C) which is assigned to nitrates, lithium entities and lattice water (calc. 34.38%). Finally, the last transition of 44.13% (350–440 °C) is assigned to the loss of the tpmc ligand (calc. 47%) and the residue of 6.5% corresponds to NiO (calc. 6.3%). These assignments are in agreement with those reported for the analogous copper–tpmc compound[36] and nickel nitrate.[37]

The thermogram of **1** exhibits a very little loss of 2.35% (≈50 °C), corresponding to 1.6 water molecules (−2.5%). This little amount of water is due to the high affinity of **1** towards water (during its manipulation, even though it is made under nitrogen). The comparison between TGA and DGA curves of **1** and **2** is shown in Fig. 12.

TGA curves of compounds **1** and **2** are the same from 200 °C to the end; this being consistent with previous findings, giving extra evidence that after heating compound **2**, this becomes compound **1**.

Additionally, the thermograms for **1** and **2** were carried out in air, as well as under nitrogen. The observed transitions were the same in both cases.

The N_2 adsorption–desorption isotherm for **1** was acquired to determine its microstructural features. Fig. S7 (ESI†) shows the resulting curve. According to the IUPAC classification,[21] it corresponds to a type IIb isotherm with a very narrow hysteresis loop, a feature that is typical for a macroporous adsorbent, which allows unrestricted multimolecular adsorption, favoured at high relative pressures. The observed hysteresis is also characteristic of a chemisorption process where a slight change in the active surface takes place.

The resulting isotherms were analysed by using the BET and BJH models.[21] According to the BET method the surface area of **1** was found to be 4.24 $m^2\ g^{-1}$, the total pore volume was 0.015 $cm^3\ g^{-1}$ and the average pore diameter was 14.48 nm. However, according to BJH analysis, the average pore diameter was aleatory distributed. Therefore, the value found by BET studies corresponds to the size of particles of the bulk solid. In order to understand this behaviour, adsorption–desorption measurements at high pressure (until 4.5 MPa), under a CO_2 flow, were performed. The resulting isotherm is shown in Fig. S8 (ESI†). A continuous increment in adsorption was observed, indicating the presence of big size pores, most probably, located in the outer layer of the compound.[38]

To obtain a deeper insight into the adsorption process, water vapour isotherms of complex **1** were obtained as a function of the humidity percentage at 303, 313 and 333 K, using nitrogen as a carrier gas (Fig. 13). The adsorption process began at the

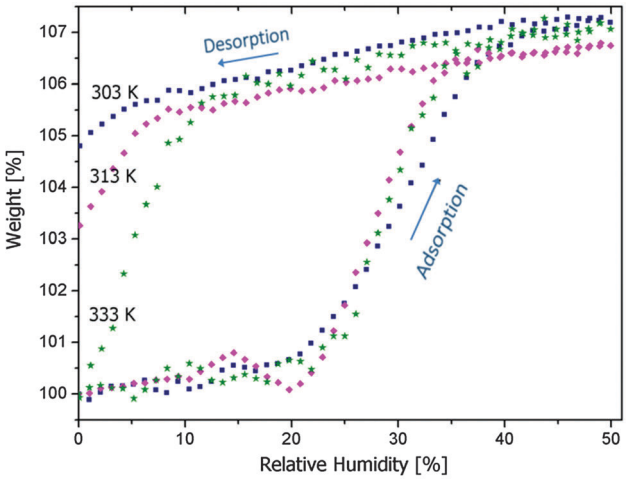

Fig. 13 Water adsorption–desorption isotherms of complex **1** measured at 30, 40 and 60 °C, using N_2 as a carrier gas.

same relative humidity percentage (RH%) and the saturation was reached almost at the same weight percentage, independently of the applied temperature. The differences between curves were the total weight gain favoured at lower temperatures. At 303 K, the maximum adsorbed water was 5 wt%, while at 313 K it was only 3 wt%. The gained weight and the fact that the curve did not end at the starting point are attributed to a chemisorption process.[21,39] In contrast, at 333 K, the curve returned to the starting point, indicating that all the adsorbed water was completely desorbed, which is characteristic of a physisorption process.[21,39] Therefore, at 333 K the energy of the chemisorption was overcome.

A second kind of water vapour isotherm measurement was performed for **1** at 303 K using different carrier gases, such as O_2 and CO_2. The corresponding curves are shown in Fig. 14. A slight increase in the maximum water adsorbed was observed when CO_2–H_2O or O_2–H_2O flows were used in comparison to the N_2–H_2O flow. This is indicative that either O_2 or CO_2 can also be adsorbed by **1**. Then, the binuclear nickel(II) compound **1** is able to adsorb carbon dioxide, dioxygen, nitrogen and water vapour,

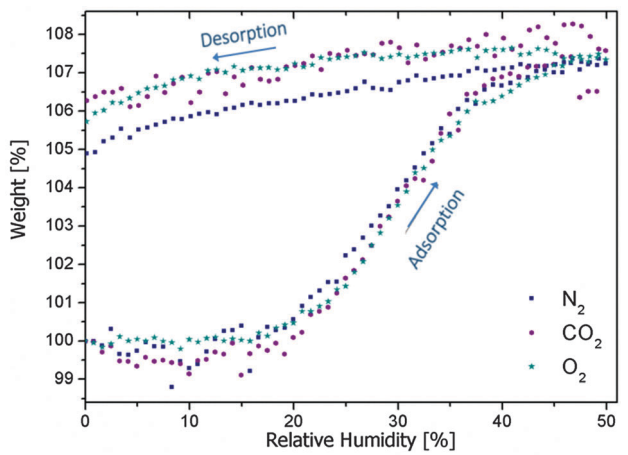

Fig. 14 Water adsorption–desorption isotherms of complex **1**, using carrier gases: N_2, CO_2 and O_2, measured at 303 K.

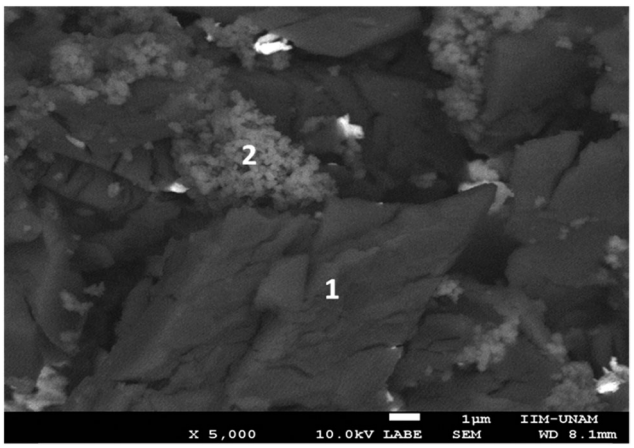

Fig. 15 Backscattered electron image of complex **2**. The different phases observed correspond to compounds **1** and **2**.

however, only the adsorption of water changes the original blue colour of **1** into the violet colour of **2**.

Interestingly, analogous compounds based on cobalt and copper, published elsewhere,[7–10,13] did not present adsorption properties, leading us to conclude that this phenomenon is inherent to nickel.[1,35]

The morphological characteristics of the binuclear nickel(II) compound, after the adsorption process, were studied by scanning electron microscopy coupled to energy-dispersive X-ray spectroscopy (SEM-EDS). Fig. 15 shows the corresponding micrographs and Fig. S9 (ESI†) shows the EDS analysis results.

Two different phases were identified. The irregular polyhedron-shaped particles were assigned to compound **1**, according to the identification by X-ray analysis and the composition determined by EDS. These dense particles, of about 10 μm, present a corrugated surface which could be associated with a large surface area and therefore with the capacity of adsorption.[40,41] The second phase is a set of small particles of about 0.1 μm corresponding to a phase rich in oxygen, which was assigned to compound **2**. The observed agglomeration is related to a small surface area, which is expected after the adsorption process took place.[40,41] Elemental percentages found by EDS agree with those found by elemental analysis (see Experimental section).

Conclusion

Two novel flexible supramolecular solids based on binuclear nickel(II) complexes with tpmc and nitrate were obtained. The blue compound **1**, $[Ni_2(tpmc)(\mu\text{-}NO_3)](NO_3)_3\,(H_2O)_2[LiNO_3{\cdot}3H_2O]$, adsorbs water leading to the violet compound **2**, $[Ni_2(tpmc)(\mu\text{-}NO_3)]_2$-$[Ni_2(tpmc)(\mu\text{-}NO_3)Li(NO_3)_2\,OH](LiOH(H_2O)_3)_2(NO_3)_8(H_2O)_{13}{\cdot}32H_2O$.

Nickel(II) ions in both compounds are in an octahedral environment, due to a non-common coordination mode of nitrate, acting as a tetradentate ligand in **1**, described as μ^2-nitrate-$1\kappa^1O,2\kappa^1O,3\kappa^2O$; while as a pentadentate ligand in **2**, described as μ^3-nitrate-$1\kappa^1O,2\kappa^2O,3\kappa^2O$. These are the first crystal structures of six-coordinated nickel(II) complexes with the tpmc ligand. It is also the first report where tpmc compounds are involved in a

reversible gas-adsorption phenomenon. The adsorption of water by **1** changes its crystal network, leading to a reversible structural phase transition, accompanied by a colour change, from the monoclinic structure of **1** to the triclinic of **2**, characterizing them as flexible supramolecular networks. This structural phase transition was also confirmed by XRPD.

Crystalline packings of **1** and **2** contain lithium entities, which play a critical role in the stabilization of the supramolecular networks. The incorporation of water induces a reaction of ligand exchange consisting of a coordination of a lithium entity towards the bridging nitrate, a process that is completely reversible when water is removed. Also the incorporation of the lithium entity into the coordination sphere of nickel in complex **2** changes its electronic environment, resulting in the observed colour change.

Two phases were identified by SEM-EDS analysis, which according to their morphology and composition were assigned to **1** and **2**.

Adsorption–desorption isotherms at low and high pressures indicated that **1** has capacity for gas adsorption. Dynamic water vapour isotherms confirm that the binuclear nickel(II) complexes adsorb water through a chemisorption process. At 333 K the chemisorption energy is overcome and physisorption takes over. Therefore, at high temperatures all adsorbed water is completely desorbed, confirming the reversibility of the adsorption phenomenon.

The binuclear nickel(II) compound **1** also has the ability to adsorb carbon dioxide, dioxygen and nitrogen, according to the isothermal measurements; nevertheless, only the adsorption of water changes the original blue colour of **1** into the violet colour of **2**, a property which might be useful for the development of molecular sensors.

Acknowledgements

We gratefully acknowledge the financial support of CONACyT, Projects 128921 and 129293, DGAPA-UNAM, Projects IN231111 and IN106014, and finally the BISNANO Project 2011. B. L. R-H. thanks CONACyT for the PhD scholarship 240230. We thank V. H. Lemus Neri, N. López Balbiaux and M. Gutiérrez Franco from USAI-UNAM (Unidad de Servicios de Apoyo a la Investigación, Facultad de Química, UNAM) for their analytical services and technical assistance; S. Barragán Rosendo from Departamento de Diseño y Medios Audiovisuales FQ-UNAM; A. Morales Espino from Laboratorio de Refinamiento de Estructuras Cristalinas (LAREC) of Instituto de Física, UNAM for his technical support; and Dr Heriberto Pfeiffer and his work group for their help with the adsorption measurements.

References

1 (*a*) R. Miyake, C. Kuwata and Y. Masumoto, *Dalton Trans.*, 2015, **44**, 2993; (*b*) M. Almasi, V. Zelenak, M. Opanasenko and J. Cejka, *Dalton Trans.*, 2014, **43**, 3730.

2 (*a*) J. Cejka, A. Corma and S. Zones, *Zeolites and Catalysis, Synthesis, Reactions and Applications*, Wiley-VCH, Weinheim, Germany, 2010; (*b*) P. Wright, M. Maple, A. Slawin, V. Patinec, A. Aitken, S. Welsh and P. Cox, *J. Chem. Soc., Dalton Trans.*, 2000, 1243.

3 (*a*) J. W. Steed and J. L. Atwood, *Supramol. Chem.*, John Wiley and Sons, UK, 2nd edn, 2009; (*b*) *Supramolecular polymer networks and gels*, Advances in polymer science, ed. S. Seiffert, Springer, Switzerland, vol. 2682015; (*c*) J. W. Steed, D. R. Turner and K. J. Wallace, *Core concepts in supramolecular chemistry and nanochemistry*, John Wiley and Sons, UK, 2007.

4 J. Boonmak, M. Nakano, N. Chaichit, C. Pakawatchai and S. Youngme, *Dalton Trans.*, 2010, **39**, 8161.

5 H. Furukawa, F. Gándara, Y. Zhang, J. Jiang, W. Queen, M. Hudson and O. Yaghi, *J. Am. Chem. Soc.*, 2014, **136**, 4369.

6 J. Narayanan, M. Sosa-Torres and R. Toscano, *J. Chem. Crystallogr.*, 2001, **31**, 129.

7 J. Narayanan, A. Solano-Peralta, V. Ugalde-Saldivar, R. Escudero, H. Hopfl and M. Sosa-Torres, *Inorg. Chim. Acta*, 2008, **361**, 2747.

8 G. Vuckovic, M. Antonijevic-Nikolic, T. Lis, J. Mrozinski, M. Korabik and D. Radanovic, *J. Mol. Struct.*, 2008, **872**, 135.

9 G. Vuckovic, E. Asato and N. Matsumoto, *Inorg. Chim. Acta*, 1990, **171**, 45.

10 N. Alcock, P. Karapulli, P. Balakrishnan and P. Moore, *J. Chem. Soc., Dalton Trans.*, 1986, 1743.

11 M. Mikuriya, I. Murase, E. Asato and S. Kida, *Chem. Lett.*, 1989, 497.

12 H. Harada, M. Kodera, G. Vuckovic, N. Matsumoto and S. Kida, *Inorg. Chem.*, 1991, **30**, 1190.

13 (*a*) B. Petkovic, M. Milcic, D. Stankovic, I. Stambolic, D. Manojlovic, V. Jovanovic and S. Sovilj, *Electrochim. Acta*, 2013, **89**, 680; (*b*) A. Ei-Motaleb and M. Ramadan, *J. Mol. Struct.*, 2012, **1015**, 56.

14 A. Vogel, *A text-book of quantitative Inorganic Analysis*, Longmans Green and Co., London, 2nd edn, 1951.

15 (*a*) *Oxford Diffraction CrysAlis CCD* and *CrysAlis RED*, Oxford Diffraction Ltd, Abingdon, England, 2010; (*b*) C. Clark and J. Ried, *Acta Crystallogr., Sect. A: Found. Crystallogr.*, 1995, **51**, 887.

16 (*a*) Bruker AXS Inc., *SAINT Version 8.27A*, Madison Wisconsin, USA, 2013; (*b*) Bruker AXS Inc., *SADABS*, Madison Wisconsin, USA, 2012.

17 G. M. Sheldrick, *Acta Crystallogr., Sect. C: Struct. Chem.*, 2015, **71**, 3.

18 (*a*) L. J. Farrugia, *J. Appl. Crystallogr.*, 1997, **30**, 565; (*b*) L. J. Farrugia, *J. Appl. Crystallogr.*, 1999, **32**, 837.

19 (*a*) C. Macrae, I. Bruno, J. Chisholm, P. Edgington, P. McCabe, E. Pidcock, L. Rodriguez-Monge, R. Taylor, J. Van de Streek and P. A. Wood, *J. Appl. Crystallogr.*, 2008, **41**, 466; (*b*) Crystal Impact Gbr, *Diamond* Version 4.0.4, Bonn Germany, 2015.

20 A. Altomare, C. Cuocci, C. Giacovazzo, A. Moliterni, R. Rizzi, N. Corriero and A. Falcicchio, *J. Appl. Crystallogr.*, 2013, **46**, 1231.

21 F. Rouquerol, J. Rouquerol, K. Sing, P. Lewellyn and G. Maurin, *Adsorption by Powders and Porous Solids, Principles, Methodology and Applications*, Academic Press, UK, 2nd edn, 2014.

22 A. P. Lever, *Inorganic Electronic Spectroscopy*, Elsevier, Netherlands, 2nd edn, 1984.
23 G. Socrates, *Infrared Characteristic Group Frequencies, Tablas and Charts*, John Wiley and Sons, UK, 2nd edn, 1994.
24 K. Nakamoto, *Infrared and Raman Spectra of Inorganic and Coordination Compounds*, John Wiley and Sons, UK, 1986.
25 A. M. Appel, R. Newell, D. L. DuBois and R. DuBois, *Inorg. Chem.*, 2005, **44**(9), 3046.
26 M. Albrecht, O. Osetska and R. Frohlich, *Dalton Trans.*, 2005, 3757.
27 N. G. Connelly, T. Damhus, R. M. Hartshorn and A. T. Hutton, *Nomenclature of Inorganic Chemistry IUPAC Recommendations 2005*, International Union of Pure and Applied Chemistry RSC Publishing, UK, 2005.
28 K. Tugashov, D. Gribanyov, F. Dolgushin, A. Smolyakov, A. Peregudov, M. Minacheva, B. Strunin, I. Tikhonova and V. Shur, *J. Organomet. Chem.*, 2013, **747**, 167.
29 S. She, Y. Chen, M. Zaworotko, W. Liu, Y. Cao, J. Wua and Y. Li, *Dalton Trans.*, 2013, **42**, 10433.
30 B. Day, J. Clayden and R. Layfield, *Organometallics*, 2013, **32**, 4448.
31 L. Pratt and A. Streitwieser, *J. Org. Chem.*, 2000, **65**, 290.
32 T. Kremer, F. Hampel, F. Knoch, W. Bauer, A. Schmidt, P. Gabold, M. Schütz, J. Ellermann and P. Schleyer, *Organometallics*, 1996, **15**, 4776.
33 G. Cakmak, J. Nuss and M. Jansen, *Z. Anorg. Allg. Chem.*, 2009, **635**, 631.
34 M. C. Etter, *Acc. Chem. Res.*, 1990, **23**, 120.
35 (*a*) R. Miyake and M. Shionoya, *Chem. Commun.*, 2012, **48**, 7553; (*b*) R. Miyake and M. Shionoya, *Inorg. Chem.*, 2014, **53**, 5717.
36 S. Sovilj, K. Babic-Samardzija and D. Minic, *Thermochim. Acta*, 2001, **370**, 29.
37 W. Brockner, C. Ehrhardt and M. Gjikaj, *Thermochim. Acta*, 2007, **456**, 64.
38 P. R. Díaz-Herrera, M. J. Ramírez-Moreno and H. Pfeiffer, *Chem. Eng. J.*, 2015, **264**, 10.
39 (*a*) H. Pfeiffer and P. Bosh, *Chem. Mater.*, 2005, **17**, 1704; (*b*) H. Mosqueda, C. Vazquez, P. Bosh and H. Pfeiffer, *Chem. Mater.*, 2006, **18**, 2307.
40 Y. Xian-Sheng, S. Miao, Z. Qin-Hui and Y. Jian-Guo, *Ind. Eng. Chem. Res.*, 2010, **49**, 6593.
41 R. Rodríguez-Mosqueda and H. Pfeiffer, *J. Phys. Chem. C*, 2013, **117**, 13452.